Tensor train based explicit multilinear modeling and control of heating systems*

Jithin Cherian[1], Enrico Uhlenberg[2], Harshith Gowda Shakaladevanapura Maregowda[3], Leandro Samaniego Vallejos[4], Torben Warnecke[5] and Gerwald Lichtenberg[6]

***Abstract*— This paper implements the concept of explicit Multilinear Time Invariant (eMTI) modeling and control of building heating systems with the help of the tensor train (TT) decomposition method. Owing to the nonlinear characteristics of building heating systems and the large number of equations required to accurately model building and radiator dynamics, the proposed novel approach employs multilinear functions in conjunction with TT algorithms as an effective black-box modeling strategy for large-scale heating systems, thus, enabling complexity reduction. Beyond parameter identification, the paper further addresses the design and the closed loop simulation of a model predictive controller that integrates this discrete-time black-box model within the supervisory control framework of a building heating system involving nine thermal radiators spanning two offices and one warehouse hall. Simulation results validate the efficacy of the proposed approach, showing it can satisfy strict user-comfort temperature bands while achieving substantial thermal energy savings.**

***Keywords:* Multilinear Systems, Tensor Decomposition, Model Predictive Controller, Tensor Trains**

I. INTRODUCTION

The energy consumption of buildings worldwide accounts for about 33% of the global energy, out of which 38% is consumed by the Heating, Ventilation and Air Conditioning (HVAC) systems. In Germany, 25.6% of the total energy is attributed to building heating systems in 2023, cf. [1], [2], with commercial buildings comprising a significant portion of it. Additionally, the maximum power demand of a building should be constrained to a value depending on the heating contract and the physical variables such as the cross section of hydraulic lines, as it incurs a high surcharge in Germany, facilitating lower energy usage in buildings. For instance, approximately 17€ per liters/hour is charged annually for the maximum power peak by the district heating network in Hamburg, Germany, see e.g. [3]. This motivates the scope of the MARGE project to develop a hierarchical model-based control concept which optimizes the energy consumption as well as the maximum power demand for heating systems while maintaining the comfort temperature band in the building. The project is conducted with the help of the Deutsches Elektronen-Synchrotron (DESY) facility in Hamburg, Germany as the demonstrator. Here, the hierarchical controller is developed to regulate the room temperatures of the offices and warehouse halls via temperature offsets, added to the reference temperatures of the rooms which are then provided to individual Proportional Integral (PI) controllers, attached to radiators.

The heating network design in buildings is often considered unique in their construction which leads to complex nonlinear models. Therefore, linear system theory cannot be used in practice, cf. [4]. A promising candidate in this field, would be multilinear systems, consisting of polynomial functions with maximum exponents of one in their monomials and hence, capture plant dynamics effectively without being overly restrictive. Furthermore, previous work has demonstrated that the nonlinear behavior of systems can be accurately approximated using an explicit Multilinear Time Invariant (eMTI) model, see e.g. [5]. This paper represents eMTI models with the help of suitable tensor decomposition methods, to derive the corresponding state-space models, cf. [6], [7], [8]. The most common type of tensor decomposition is Canonical Polyadic (CP) decomposition which is explained in [8], [9].

Also, the system model is developed using a black-box, data-driven approach, since deriving the full set of nonlinear equations for building heating systems would result in a highly complex model, thereby, increasing the computational overhead. Hence, the model is derived using the specialized Multidimensional Approximation of Nonlinear Dynamical systems (MANDy) method with real time measurement data from the building-heating systems in DESY. The MANDy method combines the data-driven approach with the Tensor Train (TT) decomposition method, see e.g. [10], [11]. The TT decomposition helps to reduce the computational costs and storage consumption of the model as opposed to various other data-driven methods. TT decomposition, unlike CP decomposition, has a higher storage demand but allows the pseudoinverse of its data tensor to be computed directly in the TT format, enabling a straightforward extraction of the parameter tensor for the state-space model, as detailed in [10], [11].

The paper is organized as follows: Section II describes the parameter identification of the TT based eMTI model and is followed by the introduction of the nonlinear model predictive controller (NMPC) in Section III. Section IV

*This paper is funded by the Federal Ministry of Research, Technology and Space (MARGE project) and the Federal Ministry for Economic Affairs and Energy (ADAPTER project) in Germany

[1]Jithin Cherian, [2]Enrico Uhlenberg, [3]Harshith Gowda Shakaladevanapura Maregowda, [4]Leandro Samaniego Vallejos and [6]Gerwald Lichtenberg are with the University of Applied Sciences, Hamburg {jithin.cherian, enrico.uhlenberg, harshith.shakaladevanapuramaregowda, leandro.samaniegovallejos, gerwald.lichtenberg}@haw-hamburg.de

[5]Torben Warnecke is with the Deutsches Elektronen-Synchrotron, Hamburg torben.warnecke@desy.de

explains the closed loop simulation results and suitable conclusions are drawn in Section V.

II. Parameter Identification

In this section, we will inspect the formulation of the states, inputs and outputs of the eMTI model in detail. For each radiator inside the building, be it inside an office or a warehouse hall, two measured signals are taken as the states and two as inputs. The first state represents the room temperature, x_k^T, measured by the thermostat attached to the radiator at time step k, while the second state corresponds to the estimated heating power, x_k^P, supplied by the radiator to raise the room temperature to the user desired comfort level. Since there is no direct measurement of this heating power, it is approximated as

$$P_i = \frac{V_{th}}{\sum_{i=1}^{n} V_i} \cdot \rho \cdot (T_{in} - T_{out}) \tag{1}$$

Variable ρ is the flow rate of the heating circuit, assigned to a specific group of radiators in the building, T_{in} and T_{out} are the inlet and outlet temperatures of the heating circuit and V_{th} is the valve position of the thermostat under consideration with n being the total number of thermostats associated with the heating circuit. The valve positions of the thermostats serve as an indicator of the total flow rate, assuming that the temperature difference between T_{in} and T_{out} provides the required thermal energy to the radiators without any significant losses.

The measured thermal power of the heating circuit is compared with the total sum of the estimated thermal powers of the radiators, associated with that circuit, to assess the accuracy and efficiency of Eq. 1, with an example provided in Section IV. Moreover, the first input represents the reference temperature of the individual PI controller, u_k^{PI}, whereas the second input is a disturbance input, u_k^D, comprising of the temperature difference between the room temperature and the environment, thus, providing an insight into the total heat loss of the room. Finally, the states and inputs of all the radiators are combined together to create the discrete-time eMTI model of the form

$$\mathbf{x}_{k+1} = \langle \mathsf{F} \mid \mathsf{M}(\mathbf{x}_k, \mathbf{u}_k) \rangle \tag{2}$$

Variables $\mathbf{x}_k \in \mathbb{R}^n$ and $\mathbf{u}_k \in \mathbb{R}^m$ denote the states and inputs of the radiators at time step k whereas n and m signify the total number of states and inputs respectively. Tensors $\mathsf{F} \in \mathbb{R}^{\overbrace{2 \times 2 \times \cdots \times 2}^{n+m} \times n}$ and $\mathsf{M}(\mathbf{x}_k, \mathbf{u}_k) \in \mathbb{R}^{\overbrace{2 \times 2 \times \cdots \times 2}^{n+m}}$ symbolize the state parameter tensor and the corresponding monomial tensor in TT format. The operator $\langle | \rangle$ represents the contracted product. More information on the tensor operations can be found in [5].

As described in [11], the parameter tensor F is derived from real-time past measurements of the states and inputs. Given t past measurements of the states and inputs where $t \in \mathbb{N}$, we create the corresponding state ($\mathbf{X}$), input ($\mathbf{U}$), and output ($\mathbf{Y}$) data matrices as

$$\begin{aligned}
\mathbf{X} &= \begin{bmatrix} \mathbf{x}_1 & \cdots & \mathbf{x}_{t-1} \end{bmatrix} = \begin{bmatrix} x_{11} & \cdots & x_{1(t-1)} \\ \vdots & \ddots & \vdots \\ x_{n1} & \cdots & x_{n(t-1)} \end{bmatrix}_{n \times (t-1)}, \\
\mathbf{U} &= \begin{bmatrix} \mathbf{u}_1 & \cdots & \mathbf{u}_{t-1} \end{bmatrix} = \begin{bmatrix} u_{11} & \cdots & u_{1(t-1)} \\ \vdots & \ddots & \vdots \\ u_{m1} & \cdots & u_{m(t-1)} \end{bmatrix}_{n \times (t-1)}, \\
\mathbf{Y} &= \begin{bmatrix} \mathbf{x}_2 & \cdots & \mathbf{x}_{t} \end{bmatrix} = \begin{bmatrix} x_{12} & \cdots & x_{1t} \\ \vdots & \ddots & \vdots \\ x_{n2} & \cdots & x_{nt} \end{bmatrix}_{n \times (t-1)}.
\end{aligned} \tag{3}$$

Next, we perform the coordinate-major decomposition of the matrices $\mathbf{X}$ and $\mathbf{U}$ mentioned in [11] and derive a matrix $\mathbf{\Psi}(\mathbf{x}, \mathbf{u})$, composed of monomial basis functions of the states and inputs from the t measurement values. For example, consider one radiator having two states x_1, x_2, and two inputs u_1, u_2, then $\mathbf{\Psi}(\mathbf{x}, \mathbf{u})$ is given by 4 where $i = 1, 2$. Subsequently, $\mathbf{\Psi}(\mathbf{x}, \mathbf{u})$ is converted into the TT format, yielding the data-driven tensor $\Psi_{\mathrm{TT}}(\mathbf{x}, \mathbf{u}) \in \mathbb{R}^{\overbrace{2 \times 2 \times \cdots \times 2}^{n+m} \times (t-1)} \equiv \mathbb{R}^{\times^{(n+m)} 2 \times (t-1)}$ and its pseudoinverse, $\Psi_{\mathrm{TT}}(\mathbf{x}, \mathbf{u})^\dagger$ is computed by the Singular Value Decomposition (SVD), cf. [11].

$$\begin{aligned}
\mathbf{\Psi}(\mathbf{x}, \mathbf{u}) &= \begin{bmatrix} \mathbf{\Psi}_{x_1} & \mathbf{\Psi}_{x_2} & \mathbf{\Psi}_{u_1} & \mathbf{\Psi}_{u_2} \end{bmatrix}, \\
\mathbf{\Psi}_{x_i} &= \begin{bmatrix} 1 & \cdots & 1 \\ x_{i1} & \cdots & x_{i(t-1)} \end{bmatrix}_{2 \times (t-1)}, \\
\mathbf{\Psi}_{u_i} &= \begin{bmatrix} 1 & \cdots & 1 \\ u_{i1} & \cdots & u_{i(t-1)} \end{bmatrix}_{2 \times (t-1)}.
\end{aligned} \tag{4}$$

To obtain a sufficiently expressive parameter tensor that captures the essential system dynamics while maintaining low computational complexity, a threshold parameter ε is tuned to truncate the singular value matrix in the SVD which helps to retain the dominant singular vectors of the system. Finally, we solve the tensor F using Eq. 5 where $\mathbf{Y}$ represents the output data matrix in Eq. 3 and the mathematical operation used here is the matrix-tensor multiplication, further explained in [11].

$$\mathsf{F} = \mathbf{Y} \cdot \Psi_{\mathrm{TT}}(\mathbf{x}, \mathbf{u})^\dagger \tag{5}$$

Figures 1 and 2 depict the parameter tensor F and the monomial tensor M for a single radiator with two states and two inputs and can be represented in TT decomposed formats $[\![\mathbf{F}_{x_1}, \mathsf{F}_{x_2}, \mathsf{F}_{u_1}, \mathsf{F}_{u_2}, \mathbf{F}_\phi]\!]$ and $\left[\!\!\left[\begin{pmatrix} 1 \\ x_1 \end{pmatrix}, \begin{pmatrix} 1 \\ x_2 \end{pmatrix}, \begin{pmatrix} 1 \\ u_1 \end{pmatrix}, \begin{pmatrix} 1 \\ u_2 \end{pmatrix}\right]\!\!\right]$ respectively. Here, $R_1, R_2, R_3, R_4 \in \mathbb{N}$ symbolizes the TT ranks described in [10]. $\mathbf{F}_{x_1}$, F_{x_2}, F_{u_1} and F_{u_2} represent the TT cores of the states and inputs and $\mathbf{F}_\phi$, the TT core of the model parameters, whose row dimension is equal to the number of states of the model. Furthermore, each element of the F tensor here, is calculated by the combined product of a row vector, three matrices and a column vector with

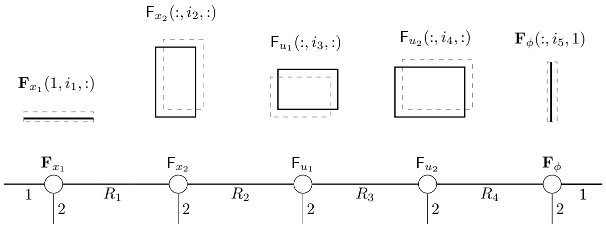

Fig. 1. Representation of the TT parameter tensor F for a single radiator

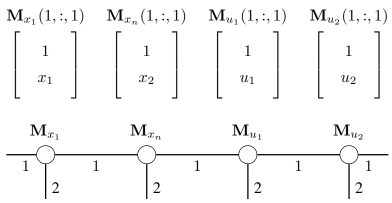

Fig. 2. Representation of the TT monomial tensor $\mathsf{M}(\mathbf{x}, \mathbf{u})$ for a single radiator

respective indices i_1, i_2, i_3, i_4, i_5 and is visually represented as thick outlines in Figure 1. F also has an additional TT core, $\mathbf{F}_\phi$, compared to M due to the fact that the contracted tensor product, $\langle | \rangle$, between F and M results in the state vector shown in Eq. 2. The TT cores of the monomial tensor M can be essentially seen as vectors, since the other two dimensions of the respective cores are set to 1. The TT cores of F and M can also be equivalently extracted from the factor matrices of the CP decomposition, see e.g. [10].

Following the construction of the parameter tensor F, the root mean square error (RMSE) value is computed between the real-time measured states and the predicted states of the model over a validation dataset in order to determine the best approximated eMTI model of the system. All the computations of the TT based parameter identification is done in Python with the help of the scikit_tt library, cf. [12].

III. Model Predictive Control

Since the TT-based eMTI model outlined in Section II is nonlinear, it leads to a non-convex optimal control problem (OCP). Therefore, an NMPC controller with a receding horizon principle is implemented, within the supervisory control framework of the heating system. Further details on the MPC development using eMTI models are provided in [10]. The closed-loop control architecture is shown in Figure 3, the general OCP in Eq. 6 and its nomenclature in Table I.

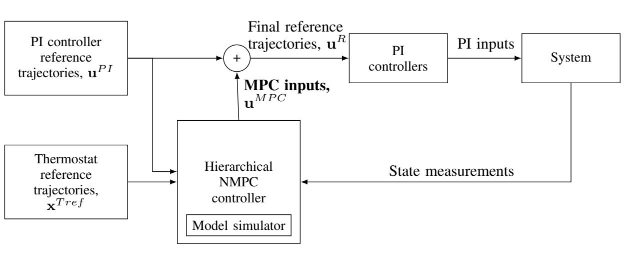

Fig. 3. Block Diagram of the MPC-based supervisory control framework

$$
\begin{aligned}
\min_{\mathbf{u}_k} \quad & J = Q\, P_k^{max} + R\, \Delta \mathbf{e}_k + S\, (\mathbf{x}_k^T - \mathbf{x}_k^{Tref})^2 \\
\text{s.t.} \quad & \mathbf{x}_{k+1} = \langle \mathsf{F} \mid \mathsf{M}(\mathbf{x}_k, \mathbf{u}_k) \rangle, \quad k = 0, \cdots, N, \\
& \mathbf{x}_0 = \mathbf{x}_{init}, \quad \mathbf{u}_0 = \mathbf{u}_{init}, \\
& \mathbf{x}_k = \begin{bmatrix} \mathbf{x}_k^T \\ \mathbf{x}_k^P \end{bmatrix}, \quad \mathbf{u}_k = \begin{bmatrix} \mathbf{u}_k^R \\ \mathbf{u}_k^D \end{bmatrix}, \\
& P_k^{max} = \max(P_{k-1}^{max}, P_k), \\
& \Delta \mathbf{e}_k = \mathbf{x}_k^P\, \Delta t, \\
& \mathbf{u}_k^R = \mathbf{u}_k^{PI} + \mathbf{u}_k^{MPC}, \\
& \mathbf{u}_k^D = \mathbf{x}_k^T - \mathbf{w}_k, \\
& \mathbf{x}_l^T \leq \mathbf{x}_k^T \leq \mathbf{x}_u^T, \\
& \mathbf{x}_l^P \leq \mathbf{x}_k^P \leq \mathbf{x}_u^P, \\
& \mathbf{u}_l^R \leq \mathbf{u}_k^R \leq \mathbf{u}_u^R.
\end{aligned}
\tag{6}
$$

TABLE I

OCP description

Nomenclature	Description	Unit
k	Current time step	-
J	Cost function	-
N	Prediction horizon	-
$\mathbf{x}_{init}$	Initial state values	-
$\mathbf{u}_{init}$	Initial input values	-
$\mathbf{x}_k$	All states of the eMTI model at time step k	-
$\mathbf{x}_k^T$	Temperature states	$°C$
$\mathbf{x}_k^{Tref}$	Temperature references	$°C$
$\mathbf{u}_k^{PI}$	PI controllers' reference trajectories	$°C$
$\mathbf{u}_k^{MPC}$	NMPC input offsets	$°C$
P_k^{max}	Total maximum thermal power	kW
$\mathbf{x}_k^P$	Thermal power states	kW
$\Delta \mathbf{e}_k$	Incremental thermal energy	kWh
Δt	Time difference between k and $(k-1)$	s
$\mathbf{u}_k$	All inputs of the eMTI model	-
$\mathbf{u}_k^R$	Final temperature reference trajectories	$°C$
$\mathbf{u}_k^D$	Disturbance inputs	$°C$
Q	Thermal power weights	-
R	Thermal energy weights	-
S	Reference tracking weights	-
$\mathbf{w}_k$	Weather	$°C$
$\mathbf{x}_l^T, \mathbf{x}_u^T$	Lower and upper bounds of $\mathbf{x}_k^T$	$°C$
$\mathbf{x}_l^P, \mathbf{x}_u^P$	Lower and upper bounds of $\mathbf{x}_k^P$	kW
$\mathbf{u}_l^R, \mathbf{u}_u^R$	Lower and upper bounds of $\mathbf{u}_k^R$	$°C$
$\mathbf{u}_l^{MPC}$, $\mathbf{u}_u^{MPC}$	Lower and upper bounds of $\mathbf{u}_k^{MPC}$	$°C$

To ensure dimensional consistency in the cost function in Eq. 6, the temperature and the thermal power states are normalized by scaling factors of $\frac{1}{100}$ and $\frac{1}{2}$ respectively. Figure 3 illustrates two reference temperature trajectories per radiator: the thermostat reference trajectory, $\mathbf{x}^{Tref}$ denote the user-defined temperature prediction of the radiator, specified in the reference tracking cost function term. The PI controller reference trajectory, $\mathbf{u}^{PI}$ exhibits a transient lead over $\mathbf{x}^{Tref}$ by 3 hours only during the rising edges, representing preheat constraints to guarantee timely tracking of the user-specified room temperature requirements and have identical values elsewhere. The thermostat and PI controller reference trajectories are shown in Figure 6 as O_ref and S_ref respectively. For each optimization cycle, the NMPC controller computes optimal input offsets $\mathbf{u}^{MPC}$, added to $\mathbf{u}^{PI}$ and forwarded to the PI controllers as final reference trajectories $\mathbf{u}^R$. Finally, the resulting PI controller inputs are applied to the radiators

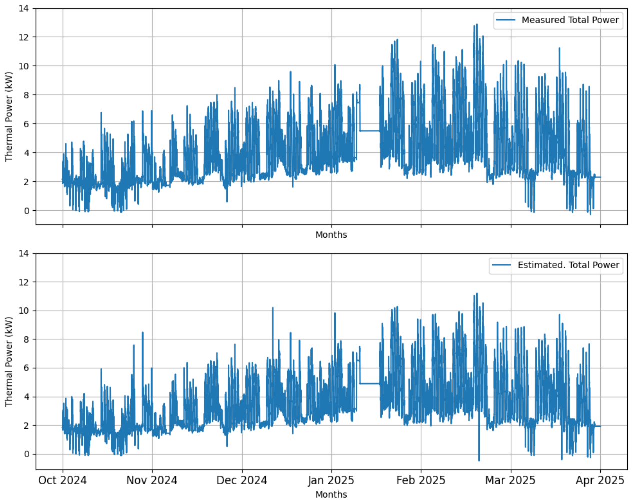

Fig. 4. Measured vs estimated thermal power of the heating circuit

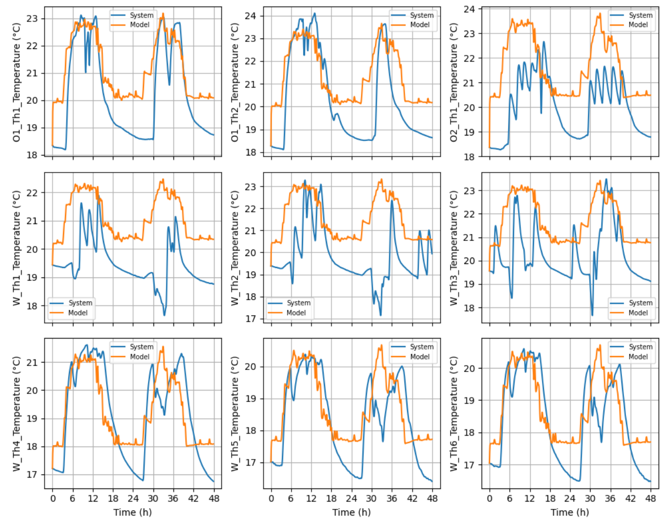

Fig. 5. eMTI model validation over 9 thermostats

TABLE II
9 THERMOSTAT eMTI MODEL

Model Properties	Value
Identification Time	$27.9s$
SVD Threshold parameter (ε)	0.035
Parameter Tensor (F) memory size	$4.12kB$
Average Room Temperature RMSE for Validation	$1.5°C$

via valve positions to regulate the room temperatures, and the updated model state measurements are subsequently fed back to the NMPC controller. The model simulator depicts the TT-based eMTI model defined in Section II. The closed-loop simulation of the system is implemented in Python using the CasADi library together with the Interior Point Optimization (IPOPT) framework, cf. [13], [14].

IV. Simulation Results

In this section, the proposed eMTI model is developed from the real-time data of building heating systems, using the MANDy method and the corresponding closed loop simulation results are presented.

A. Validation of thermal power estimation

As mentioned in Section II, the validation of the estimated thermal power of the heating circuit is performed using real-time measurements, including flow rate, inlet and outlet temperatures of the circuit, and valve position data from 74 radiators heated by the circuit. The goal is to compute the estimated thermal power of each individual radiator using Eq. 1 and add them up to compare the total estimated quantity with the measured real-time thermal power of the circuit over the winter months from October 1, 2024 until March 31, 2025 and the result is shown in Figure 4. The RMSE value between the measured and the estimated thermal power of the heating circuit during this period is $0.6kW$.

B. System model validation

The eMTI model used for the closed-loop simulation consists of nine thermostats: three associated with two offices, and the remaining six assigned to a warehouse hall. The parameter identification process described in Section II, is utilized over a 13-day training period with measurements sampled every five minutes and the model accuracy is validated over an additional 2-day period. Figure 4 illustrates the accuracy of a good-fit model across all nine thermostats, evaluated from the room-temperature perspective. In this figure, the first row corresponds to the office thermostats (O - Office, Th - Thermostat) and the last two rows refer to the warehouse hall thermostats (W - Warehouse hall). More details about the model is given in Table II. The threshold parameter (ε) tuning criterion is performed by comparing the values of two quantities, namely the overall mean RMSE value of the states and the size of the parameter tensor, over a range of threshold values. Also, the threshold values above 0.035 lead to the omission of critical system dynamics while values below 0.035 causes overfitting of the model in addition to higher model sizes and computational times.

C. Simulation analysis

Closed loop simulations are performed using the TT-based eMTI model and the NMPC controller over a span of 2 days with suitable cost function weights and constraints demonstrated in Table III. Here, the value of P_k^{max} is set initially as the maximum thermal power of the model obtained over the same simulation period without the NMPC, P_0^{max}. Also, the value of the reference-tracking cost-function weight S in Eq. 6 is dynamically assigned at each iteration based on the temperature difference between the room and the reference temperatures for each thermostat. Specifically, S is set to 0 when the room temperature exceeds the reference temperature, otherwise it takes the value specified in Table III, a concept known as zone control or funnel MPC, cf. [15]. This is done due to the persistent underheating observed in the past temperature measurements of all thermostats in the building, where the room temperature

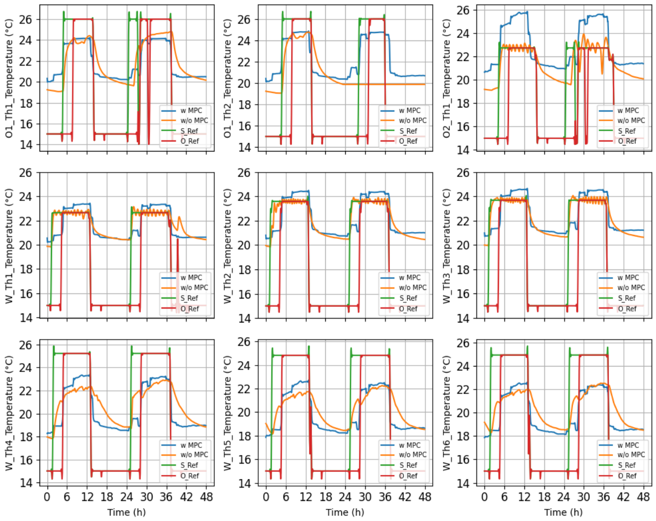

Fig. 6. Closed loop simulation of room temperatures

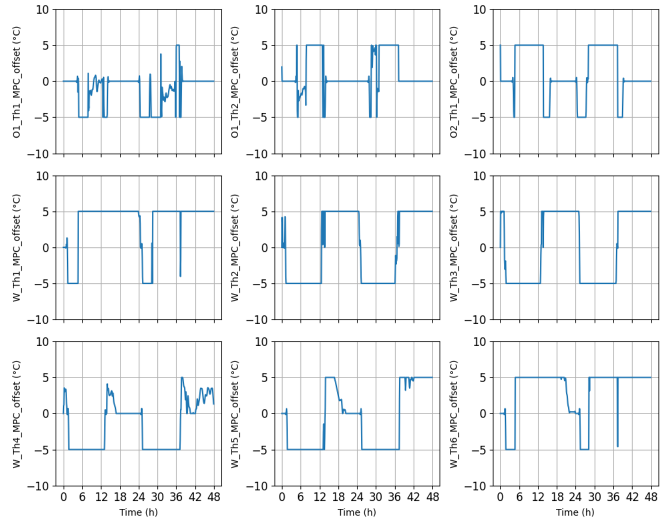

Fig. 7. MPC input offsets of the closed loop simulation

consistently fails to reach the reference temperature by a few degrees because of heat losses. Also, during unoccupied periods, the thermostat occupancy sensor triggers a drop in the thermostat reference temperature to a minimum of $15°C$. Consequently, the comfort weight S is set to zero, ensuring that the power and the energy weights become dominant in the NMPC objective function, leading to negative NMPC inputs. The simulation results of the nine thermostats can be seen in Figures 6, 7 and 8. All simulations were conducted on a 64-bit operating system featuring an Intel (R) Core (TM) Ultra 7 155U (1.70 GHz) processor and a 32 GB RAM.

TABLE III

COST FUNCTION WEIGHTS AND CONSTRAINTS

Cost function weight	Value
N	3 *hours*
Q	171.12
R	100.35
S	1000
$[\mathbf{x}_l^T, \mathbf{x}_u^T]$	$[15, 30]°C$
$[\mathbf{x}_l^P, \mathbf{x}_u^P]$	$[0, 2]kW$
$[\mathbf{u}_l^{MPC}, \mathbf{u}_u^{MPC}]$	$[-10, 10]°C$
Range of $\mathbf{w}_k$	$[5.5, 10.5]°C$
P_0^{max}	$2kW$

In Figure 6, the blue and orange curves represent the room temperatures with and without the MPC respectively, while the red curves correspond to the original thermostat reference temperature (O_Ref), and the green curves represent its shifted version (S_Ref). Also, the underheating trend of the radiators can be seen from Figure 6. In Figure 8, the left side subplots refer to the simulation period without the MPC supervisory control and the right side subplots indicate the same period with the MPC control.

D. Performance Evaluation: With vs. Without MPC

In this section, the overall effectiveness of the MPC is examined for the closed loop simulation with reference to Figures 6, 7 and 8.

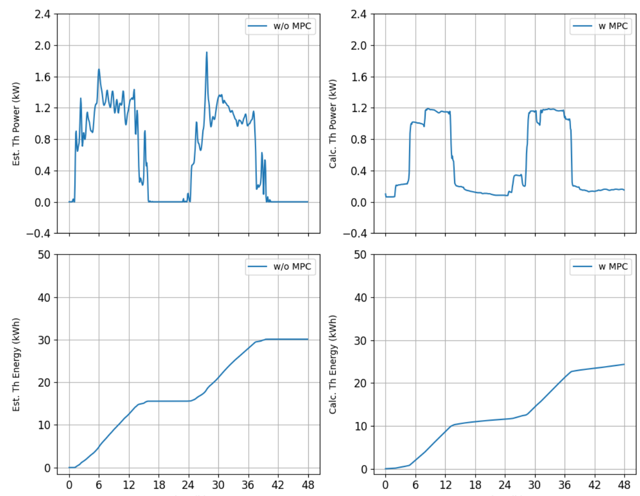

Fig. 8. Thermal power and energy simulation results

- The MPC effectively regulates the room temperatures closer to their respective references, compared to the non-MPC simulation, see Figure 6. Furthermore, during the 3-hour preheat duration preceding the scheduled rise to the user comfort temperature, the MPC constrains the room temperatures to remain below their reference values by providing negative offsets. This behaviour demonstrates the controller ability to prevent unnecessary overheating, thus, saving thermal energy. Also, during the scheduled descent from the user comfort temperature towards the minimum comfort temperature, the MPC controller introduces negative offsets, prior to the actual descent while keeping the room temperatures close to its references, contributing to energy efficiency.
- In Figure 6, the subplots in the first row represent two neighboring offices, with a small open passage between the rooms. Here, the room temperature in the third

subplot exceeds its reference by approximately $3°C$. This behaviour is consistent with the MPC operation, as the controller interprets the eMTI model and establishes temperature relationships among different thermostats. In this case, the MPC utilizes only two of its three input offsets to control the three office radiators, while keeping the third offset as low as possible. Figure 7 illustrates the MPC input offsets for all nine thermostats, highlighting this allocation strategy.

TABLE IV
COMFORT BAND VS ENERGY EFFICIENCY

S value	$\mathbf{x}_k^T - \mathbf{x}_k^{Tref}$	Max. TP ↓	Total TE ↓	Total cost ↓
200	$[-5, 1]°C$	57%	50%	57%
500	$[-4, 2]°C$	36%	40%	36%
1000	$[-3, 3]°C$	14%	17%	14%

- The NMPC significantly reduces the thermal power and energy consumption while maintaining the prescribed comfort bounds, see Figure 8. Without the MPC control, the nine radiators have a peak thermal power demand of approximately $1.4kW$, see first subplot of Figure 8. Values exceeding this threshold are due to measurement noise spikes in the flow-rate sensor of the heating circuit. Table IV provides an overview of the trade-off between the comfort band at the user-defined temperature $\mathbf{x}_k^T - \mathbf{x}_k^{Tref}$ and the energy efficiency across varying cost weights S. Here, TP is thermal power and TE, thermal energy. For all tested S values, the difference between the room temperatures, with and without the MPC, remained within a tolerance of $\pm 1°C$.
- The maximum NMPC computational time for the OCP presented in Eq. 6 is close to $30s$ (maximum 50 solver iterations per time step) which is fast enough to ensure reliable temperature regulation with minimal operational criticality. Also, the NMPC solver has a hard constraint to ensure that it provides an input under every 5 minutes by capping the maximum number of solver iterations per time step to 200. If the solver reaches the maximum number of iterations before finding an optimal solution, it returns the best feasible iterate and in the event of a solver failure, it defaults to suitable inputs from the previous optimal trajectory until an optimal solution is found. The IPOPT framework in CasADi requires the Jacobian matrix of the TT-based eMTI model to construct the linearized sub-problems of the OCP, see [16]. The novel linearization method for the TT-based eMTI model, cf [17], is the principal contributor to such low NMPC computational times.

V. CONCLUSIONS AND FUTURE WORK

This paper proposes a methodology to multilinearize a non-linear building heating system explicitly with the help of TT decomposition. In the model design phase, past signal measurements are retrieved and processed using the MANDy modeling strategy. The result yields an explicit multilinear model encoded in the Tensor-Train decomposition format due to its significant advantage in computing the pseudoinverse of the data tensor. The final model is determined by evaluating the RMSE values that capture the modeling error between the measured and predicted signals on a validation dataset, with an SVD threshold parameter used to ensure numerical robustness.

After the construction of the model, the MPC controller is developed within the supervisory control framework for the building heating systems. The application of the introduced method on a simulated heating system example shows the advantages of the approach over a non-supervisory framework including improved comfort bands and higher gains on energy savings. The future work of this project will focus on real time experimental testing within a DESY facility.

REFERENCES

[1] Umweltbundesamt, "Indicator: Energy consumption for buildings," 2025, accessed: 24.11.2025. [Online]. Available: https://www.umweltbundesamt.de/en/data/environmental-indicators/indicator-energy-consumption-for-buildings

[2] M. González-Torres, L. Pérez-Lombard, J. F. Coronel, I. R. Maestre, and D. Yan, "A review on buildings energy information: Trends, end-uses, fuels and drivers," *Energy Reports*, vol. 8, pp. 626–637, 2022.

[3] H. Energiewerke, "Costs & prices city network," 2025, accessed: 24.11.2025. [Online]. Available: https://www.hamburger-energiewerke.de/waerme/fernwaerme-stadtnetz/kosten-preise

[4] V. Harish and A. Kumar, "A review on modeling and simulation of building energy systems," *Renewable and Sustainable Energy Reviews*, vol. 56, pp. 1272–1292, 2016.

[5] K. Kruppa, G. Pangalos, and G. Lichtenberg, "Multilinear approximation of nonlinear state space models," *IFAC Proceedings Volumes*, vol. 47, no. 3, pp. 9474–9479, 2014, 19th IFAC World Congress.

[6] W. Hackbusch, *Tensor Spaces and Numerical Tensor Calculus*, 2nd ed. Springer, Cham, Switzerland, 2019.

[7] G. Lichtenberg, "Hybrid tensor systems," Ph.D. dissertation, University of Technology, Hamburg, 2011.

[8] G. Pangalos, A. Eichler, and G. Lichtenberg, "Tensor systems: multilinear modeling and applications," in *Proceedings of the 3^{rd} International Conference on Simulation and Modeling Methodologies, Technologies and Applications : Reykjavík, Iceland, 29 - 31 July, 2013*, 2013, pp. 275–285.

[9] T. G. Kolda and B. W. Bader, "Tensor decompositions and applications," *SIAM Review*, vol. 51, no. 3, pp. 455–500, 2009.

[10] K. Kruppa, "Multilinear design of decentralized controller networks for building automation systems," Ph.D. dissertation, HafenCity University, Hamburg, 2018.

[11] P. Gelß, S. Klus, J. Eisert, and C. Schütte, "Multidimensional approximation of nonlinear dynamical systems," *Journal of Computational and Nonlinear Dynamics*, vol. 14, no. 6, 2019.

[12] P. Gelß, A. Ramos, T. Bake, H. D. Nguyen, M. Lücke, D. S. Klus, M. Scherer, and D. F. Nüske, "scikit_tt," 2025, accessed: 26.11.2025. [Online]. Available: https://github.com/PGelss/scikit_tt

[13] J. A. E. Andersson, J. Gillis, G. Horn, J. B. Rawlings, and M. Diehl, "CasADi – A software framework for nonlinear optimization and optimal control," *Mathematical Programming Computation*, vol. 11, no. 1, pp. 1–36, 2019.

[14] Y. Kawajir, C. Laird, and S. Vigerske, "Ipopt documentation," 2025, accessed: 26.11.2025. [Online]. Available: https://coin-or.github.io/Ipopt/

[15] S. Prívara, J. Široký, L. Ferkl, and J. Cigler, "Model predictive control of a building heating system: The first experience," *Energy and Buildings*, vol. 43, no. 2, pp. 564–572, 2011.

[16] A. Wächter, "Short tutorial: Getting started with ipopt in 90 minutes," in *Combinatorial Scientific Computing, 01.02. - 06.02.2009*, U. Naumann, O. Schenk, H. D. Simon, and S. Toledo, Eds., vol. 09061. Schloss Dagstuhl - Leibniz-Zentrum für Informatik, Germany, 2009.

[17] J. Cherian and G. Lichtenberg, "Efficient linearization for explicit multilinear models in tensor train representation," 2026, accepted to the 12^{th} CoDIT Conference 2026.